缺損修復演算法在

頭顱骨修復技術之研究

The Research of Skull Prosthesis through

Defect Repairing Algorithm

中華民國一百零六年六月

ABSTRACT

Keywords: Prosthesis, Tomography, Geometric Modeling, Active Contour Models, Differential Evolution algorithm

Skull defects can lead to risk of brain infection, low brain protection situation, and mental social barriers. In order to avoid these situations, we must build a prosthesis and transplant it to the defect area. With the development of Additive Manufacturing and 3D printing technology, skull prosthesis can be manufactured precisely and efficiently during skull reconstruct surgery. However, the skull prostheses made by the metal implants are not always in full compliance with the needs of the defective area. Unsuitable prosthesis may cause repeated brain infections and require secondary surgery. This study proposes a Differential Evolution Algorithm and an Active Contour Models to construct suitable skull prosthesis. It can be adjusted in each tomography slice according to the graphic features. The proposed method can model the defective region of the skull defect, and the resulting pattern can fully simulate and compensate for the skull defect area. So that clinical surgeons can implant the prosthesis very quickly into patient, especially in emergency surgery. This study can solve the problem of skull defects, so that patients can get the best help in surgery.

Chapter 1 Introduction

Skull defects can be divided into two types, birth defects and acquired damaged. Birth defect usually occur at birth, such as congenital malformations. Acquired damaged usually occur in patients with trauma or decompressive craniectomy (Aarabi et al., 2006; Cooper et al., 2011; Josan et al., 2005; Rish et al., 1979; Taggard & Menezes, 2001). When patients with skull defects will cause a significant impact, the external protection of brain is reduced and the metabolism of brain tissue is also influenced (Kuo, Wang, Chio, & Cheng, 2004; Winkler, Stummer, Linke, Krishnan, & Tatsch, 2000). In addition, the appearance of the incomplete skull also causes the patient appearance integrity, psychological stress, frustrated, and crowd social barriers. Therefore, the reconstruction of the skull is an important issue in physiological function and psychological condition of the patients In order to reconstruct skull defects, cranioplasty is a common operation in clinical. Cranioplasty recover the defects using size and shape matched bone flaps (Gooch, Gin, Kenning, & German, 2009; Sanan & Haines, 1997). Currently, many types of skull bone flaps have been developed and applied in clinical, such as autografts, allograft, xenograft and synthetic bone. From the point of view of infection and immunity, the autografts have a low risk of infection and immune response (Black, 1978). The bone flaps used to repair the defects are usually removed or modified from tibia and rib bones (Taggard & Menezes, 2001; Viterbo, Palhares, & Modenese, 1995). However, the autografts have some problems during the surgery. Before the implantation, the autografts need to be preserved well and then it require adequate blood perfusion after cranioplasty. Therefore, the autografts are usually unavailable in clinical, especially in an emergency situation. Allogeneic and xenogeneic bone flaps are usually obtained from cadavers or animals. Allogeneic and xenogeneic bone flaps have the advantage of being able to be cultured in advance. However, due to the high risk of infection and rejection, allografts and xenografts are rarely used in clinical or practical case (Gruber, Peter, & Hora, 1988; Prolo & Oklund, 1991).

Bone cement is another material commonly used in clinical to repair and strengthen patient’s bones. Bone cement is not like autografts which needed to obtain from tibia and rib bones. It can be arbitrary shaping and has the advantages of rapid solidification and cheap (Liebschner, Rosenberg, & Keaveny, 2001). Bone cement has been widely applied in bone surgery, such as, vertebroplasty (Deramond, Wright, & Belkoff, 1999; Lewis, 1997), hip-joint replacement (Jiranek, Hanssen, & Greenwald, 2006) and cranioplasty (Plum & Tatum, 2015). However, bone cement needs to be manual shaping during cranioplasty operation, which

prolongs the operation waiting time and increase the risk of infection and surgical complications. In addition, shaping the bone cement manually is subjective and is difficult to maintain the symmetry of the head, surface fit, and smoothness of bone flaps. In recent years, with the medical imaging and additive manufacturing (AM) have been widely and rapidly developed, the anatomical structural information of patient, such as skull bone, can be accurately acquired using high-resolution computed tomography (CT) (Ghadimi, Moghaddam, Grebe, & Wallois, 2016; Liacouras, Garnes, Roman, Petrich, & Grant, 2011; Sahillioğlu & Kavan, 2015). Bone flaps can be designed on the basis of the CT images to fit defective part and can be further produced using additive manufacturing techniques. By shortening total operation time and accurate bone flaps the quality of cranioplasty can be improved. However, using bone cement to model bone flap still relies on manual designs by clinical engineers currently. This bone flap modeling procedure and design could take several hours or even days depending on the experience of engineers. Eventually, the operation may be delayed, so it is usually not feasible in the emergency situation.

In this study, we proposed two novel algorithms to automatically model the skull defects and compare to each other. We solved the bone flap modeling procedure manually problem by using algorithms to find the suitable bone flap automatically. We dramatically reduce operating time and make it feasible on emergency situation.

Chapter 2 Literature Review

2.1 Current classification method

In the literature, several computational methods and mathematical methods relying on CT images for defining and designing prosthesis have been developed for the purpose of repairing skull defects (Rudek, Gumiel, & Canciglieri Jr, 2015; Sahillioğlu & Kavan, 2015; Zhou et al., 2013). These methods include the mirroring technique (Maravelakis et al., 2008), surface fitting (Chong, Lee, & Kumar, 2006), or formed templates (Dean & Min, 2003). These methods can be classified as two types: skull template registration (Liao et al., 2011; Liao et al., 2013; Wagner et al., 2015) and parametric model fitting (Huang & Shan, 2011; Z. Zhang, Zhang, & Song, 2014).

In skull template registration, series of complete skull CT images are used as a template and aligned to the CT images of subsequent defects using image registration or image deformation. These series of complete skull CT images are acquired before a defect occurs. After the registration, the skull defects are intrinsically repaired and modeled similarly with the

original in the registered images. However, complete skull CT images acquired for skull template registration are rarely available in urgent clinical practice. In addition, the accuracy of the defects area needed to be modeled depends on the quality of the image registration results. Even in a well-converged skull template registration condition, the registration results usually include mismatch errors, subsiding problem, or protruding problem, which undermine the accuracy of the modeled defects. Moreover, the computational complexity and calculating time involved in the registration of such high-resolution CT images is considerable. To reduce calculating time, however, CT images can be transformed into scale spaces using a Gaussian pyramid or a wavelet transform by following a coarse-to-fine multi-resolution image registration. But mismatch errors could still exist in low-scale registration and even increase in high-scale registration.

Parametric model fitting could be used to repair skull defects without the need for reference images in skull template registration. After a mathematical parametric model is defined, the missing skull surface is generated by fitting the remaining cranial surface information of the skull bone. By using mathematical parametric model fitting, a surface fitting in 3D volumes can be achieved through the same concept in 2D images. Among the most common used surface-fitting methods are the Bézier surface (Chong et al., 2006) and the radial basis function (Carr, Fright, & Beatson, 1997). The curve and edge of the fitted skull surface (prosthesis) are reach the requirement or not depend on the applied models and their parameter settings. Although the missing skull surface can be obtained in a single 3D fitting, the parameters still need to be adjusted to account for the surface shapes and curvatures in different cranium areas, which is a complex and time-consuming problem, also to account for individual dependence. The use of 3D fitting without additional constraints may produce abnormal subsiding or protruding areas problem in the fitted skull surface. By contrast, the curve fitting in 2D images is less complex in both the parameter settings and the fitting computation. With a proper mathematical parametric model, parameter settings, and high resolution CT images, the curve fittings generally produce appropriate surfaces for the defect modeling.

As mentioned above, the parameters need to be adjusted manually in parametric model fitting still need to be resolved. In different case surface shapes and curvatures of cranium areas, parameter settings should be different according to the conditions. It is a complex and time-consuming problem. There are other ways to solve this problem. We can use the algorithm to automatically find the parameters to save the manual adjustment of time-consuming (Greboge, Rudek, Jahnen, & Júnior, 2013; Rudek et al., 2015). Evolutionary algorithms (EAs) (Back,

Fogel, & Michalewicz, 1997) were inspired by animal behavior pattern, and many variant meta-heuristic algorithms developed from this similar concept, such as the Genetic Algorithm (GA)(Davis, 1991) and the Particle Swarm Optimization Algorithm (PSO)(Kennedy, 2010). In several studies, EAs and parametric model fitting have been integrated and used to solve broken skull reconstruct optimal problems (Greboge, Grebogi, Rudek, & Canciglieri Jr, 2011; Junior, Rudek, & Greboge, 2011).

Rudek, Greboge, Coelho, and Canciglieri Jr (2011) overcome the shortcoming in traditional mathematical approaches, for example, the initial solution affect convergence dependency and problem-solving inefficiency because of the discrete search spaces. They used GA to evaluate the parameters in the ellipse function, which is a method that can be used to generate different sizes and types of ellipses to fit the skull. Rudek, Canciglieri Jr, and Greboge (2013) noted that the mirror image concept is a common method can be adapted for most skull reconstruction problems except when the defects are through the center line of the head (forehead or back of the head)(Li, Xie, Ruan, & Wang, 2009; Sengupta, Sengupta, & Ghosh, 2005). In order to get over asymmetric skull prosthesis issues, they used PSO (Kennedy, 2010) and superellipse to conquer this problem.

Overall, many researches have solved skull-repair problems by using algorithms. Among one of the popular meta-heuristic algorithms, Differential Evolution (DE), was proposed by (Storn & Price, 1997). DE is well known as a population-based stochastic search technique, adapts fewer parameters, and retains the diversity of the population. In this present study, we apply DE methodology, because compare with other EAs it is more reliable, better performance, and converges more rapidly in solving optimal problems (Hu, Xiong, Su, & Zhang, 2013; Salman, Engelbrecht, & Omran, 2007). On the other hand, there is another algorithm active contour models, also called Snakes, which is widely used in the field of image processing algorithms. Snakes can be used on the issue of skull repair due to it is good at finding the boundaries or endpoints in the image. This study applied DE and Snakes in skull defect repair and comprehensive discuss their advantages and disadvantages. Other details of the algorithms are show as section 2.3 and section 2.4.

2.2 Superellipse Definition

From the perspective of skull anatomy, although most shapes of the skull as shown in each CT layers is approximate oval, they are by no mean the same (Rudek et al., 2013). Therefore, that means the bone in each CT image can be modeled as various kinds of oval shapes. Superellipse has this feature to fulfill all the requirements of skull modeling. Superellipse is a variable mathematical model can be used to create any geometry commonly found in nature

(Gielis, 2003; Spehr, Gumhold, & Fleming, 2011; X. Zhang & Rosin, 2003). The mathematical formulation of the Superellipse is presented in Equation (2.1).

$$r(\varphi) = \frac{1}{\sqrt[n1]{\left(\left(\left|\frac{1}{a}cos(\frac{m}{4}\varphi)\right|\right)^{n2} + \left(\left|\frac{1}{b}sin(\frac{m}{4}\varphi)\right|\right)^{n3}\right)}} \quad (2.1)$$

The parameter a and b respectively represent the major axis and minor axis of the generated shape. The m value is the number of fixed arguments on the generated shape. The shape obtained from this equation (2.1) is a quadrilateral shape when m=4 and a circle when m= 0. The values of $n2$ and $n3$ affect the smoothness of the shape and determine whether the shape is inscribed or circumscribed in a unitary circle (Rudek et al., 2013).

In Figure 1, with the different values of the Superellipse parameters we can obtain different polygons. The polygon in Figure 1(a) and Figure 1(b) have four fixed points (m =4) and three fixed points (m=3). They look like a quadrilateral and looks like a triangle respectively. Figure 1(a), Figure 1(c) and Figure 1(d) have the same m value (m=4). However, in these cases, the borders are irregular because of the modified n values. The parameter n determines the curvature of the equation and can make it taut or twists and turns. Traditionally, an ellipse can be obtained when $n1$= $n2$= $n3$= 2 and m=4, and in this parameter setting we have the ellipses equation. By observation, the shape of some CT slices in the top and middle of the skull are similar with a normal ellipse. When the shape becomes more oval, we can auto fit the skull by adjusting the values of n in Superellipse.

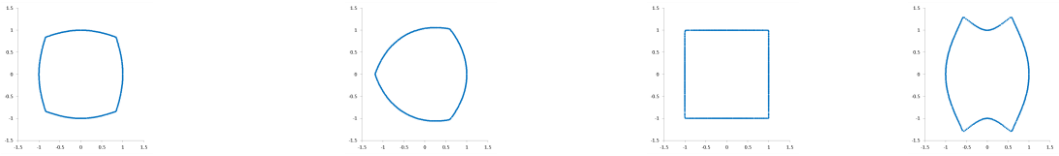

(a) (b) (c) (d)

Figure 1 Examples for different Superellipse parameters (a) [a=1, b=1, m=4, $n1$=200, $n2$=100, $n3$=100]; (b) [a=1, b=1, m=3, $n1$=200, $n2$=100, $n3$=100]; (c) [a=1, b=1, m=4, $n1$=100, $n2$=100, $n3$=100]; (d) [a=1, b=1, m=4, $n1$=50, $n2$=20, $n3$=200]

2.3 Differential Evolution Algorithm

The Differential Evolution (DE) algorithm is a population-based meta-heuristic algorithm proposed by Storn and Price (1997) and compare with other EAs it is perform better, and converges more rapidly in solving optimal problems (Hu et al., 2013; Salman et al., 2007). The position of an individual in a population represents a combination of decision variables as a solution of the objective function. An individual (i) in one population for each generation (G)

is represented by a *D*-dimensional vector, shown as $X_{i,j,G} = (X_{i,1,G}, X_{i,2,G}, \ldots, X_{i,j-1,G}, X_{i,D,G})$. A population consists of NP individuals, i=1,2,…, *NP*. *G* denotes one generation. (G_{max}) represents maximum number of generations and it is also a stopping criterion for the DE's search procedure. The procedure of DE consists of three operations: the mutation operation, the crossover operation, and the selection operation (Storn & Price, 1997). The main operations of the classic DE are shown as follows:

(1) Mutation: The main purpose of mutation operation is used to generate a new individual as a mutation vector (*V*). Mutation vector is the combination of three randomly chosen individuals in the current population, as shown in Equation (2.2).

where $r1, r2, r3 \in \{1,2, \ldots NP\}$ are random differ integers, each of which differ in accord with index i. The scaling factor F controls the scale of difference between $X_{r2,G}$ and $X_{r3,G}$ which is a real and constant factor $\in [0,2]$.

$$V_{i,G+1} = X_{r1,G} + F \cdot (X_{r2,G} - X_{r3,G}), r1 \neq r2 \neq r3, \quad (2.2)$$

(2) Crossover: After doing mutation operation do crossover operation. The crossover operation represents the exploitation ability of individuals. The crossover operation generates the trial vector ($U_{i,G+1}$) from the target vector ($X_{i,G}$) and the mutation vector ($V_{i,G+1}$) by using probability decision in classic DE. The value of dimension *j* of the trial vector is decided from target vector or mutation vector according to the random number of dimensions *j* ($rand_j$), as shown in Equation (2.3):

$$U_{i,j,G+1} = \begin{cases} V_{i,j,G+1}, if\ rand_j \leq CR \\ X_{i,j,G}, otherwise \end{cases}, \quad (2.3)$$

where j denotes the dimension. i and G^{th} denote individual and iteration respectively as mentioned before. The larger the *CR* value, the higher probability trial vector chosen from mutation vector.

(3) Selection: Selection operation is a greedy strategy, as showed in Equation (2.4). If and only if the fitness of trial vector ($U_{i,G+1}$) is better than the fitness of target vector ($X_{i,G}$), the trial vector ($U_{i,G+1}$) will become the next generation target vector ($X_{i,G+1}$). Otherwise, the old target vector ($X_{i,G}$) is retained:

$$X_{i,G+1} = \begin{cases} U_{i,G+1}, if\ f(U_{i,G+1}) \leq f(X_{i,G}) \\ X_{i,G}, otherwise \end{cases} \quad (2.4)$$

These three operation (Mutation, Crossover, and Selection) will continue to evolve repeatedly until individuals reach the stop condition or the maximum number of generations.

2.4 Active Contour Models Definition

Active contour models is also called Snakes. It is a strategy of evolving curves driven by minimizing the internal and external energies (Kass, Witkin, & Terzopoulos, 1988) as shown in Equation (2.5).

$$E_{snake} = \int_0^1 E_{snake}(v(s))ds = \int_0^1 E_{int}(v(s)) + E_{image}(v(s)) + E_{con}(v(s))ds \qquad (2.5)$$

where $v(s) = (x(s), y(s))$ represents the position of each point in snakes parametrically; In equation (2.5), energy can be categorized into two parts, internal and external energies. Among, E_{int} is the internal energy of a spline caused by bending. The remaining two, E_{image} is the force of the spline which guide the spline moving toward the lines, edges, and terminations in the image; and E_{con} gives rise to external constraint forces.

Internal energy can make the Snakes contour tense and stiff. External energy derived from the image features guides the Snakes contour toward the region of interest (Liao et al., 2013). Combine the characteristics of these two energies, Snakes can effectively find the image location. The objective of snakes is to minimize the internal and external energies for deriving the Euler–Lagrange equation as shown in Equation (2.6):

$$\alpha v'' + \beta v'''' + \frac{\partial E_{ext}}{\partial v} = 0 \qquad (2.6)$$

where v denotes the coordinate vector of the contour with entities v_i, for $i = 1, 2, \ldots, N$ (N is the total number of vertices in Snakes). The leading two parts of the equation $\alpha v'' + \beta v''''$ represent the internal energy of Snakes. The leading two terms coefficients α and β control the tension and stiffness of the generated curve. The last part of the equation $\partial E_{ext}/\partial v$ represents the external energy of Snakes. The external energy forces the curve moving toward the lines, edges, and terminations in the graphic.

After using a finite difference to approximate derivatives, the Euler–Lagrange equation becomes Equation (2.7). This expansion equation can be rewritten into a matrix form: $A_v + f_v = 0$, where A is a matrix consisting of α and β, and f_v is associated with external energy. A can be solved using matrix inversion. The details of the decomposition methods for Snakes are provided by (Kass et al., 1988).

$$\begin{aligned} &\alpha_i(v_i - v_{i-1}) - \alpha_{i+1}(v_{i+1} - v_i) + \beta_{i-1}(v_{i-2} - 2v_{i-1} + v_i) \\ &\quad - 2\beta_i(v_{i-1} - 2v_i + v_{i+1}) + \beta_{i+1}(v_i - 2v_{i+1} + v_{i+2}) + f_v(i) = 0 \end{aligned} \qquad (2.7)$$

Chapter 3 Proposed Method

In cranioplasty, the main purpose of a prosthesis is to repair defects of the skull bone. The prosthesis reconstruction strategy flowchart was illustrated in Figure 2. The main steps in the flowchart comprised medical image data processing, fitting curve calculation on 2D tomography, 3D modeling construction, and 3D printing.

The first step is image pre-processing. In this step, we acquire and process computed tomography images (CT) then that can be used in the next step. CT images are cut into multiple layers of the head and scanned into a picture file. In this study, all medical tomography images were extracted in the Digital Imaging and Communications in Medicine (DICOM) file format. In this step, some noises such as brain or other soft tissues are eliminated from the CT images and we can acquire the whole solid bone graphic. After filtering out the skull bone region, only the inner and outer borders are used for the next step.

The second step is the reconstruction behavior of the geometrical model of the missing skull bone by using combination of parametric model fitting and algorithm. The main purpose in this step is to reconstruct missing skull bone in every 2D CT. Suitable arcs can be identified using combination of parametric model and algorithm. The fitting details are shown in Section 3.1 and Section 3.2.

In the third step, all layers of processed CT images in the first and second step are integrated to build a 3D visualization of the skull. 3D visualization of the skull can be visualized by stacked CT images together. The cranial prosthesis can be visually validated. Suitability of the prosthesis is confirmed by medical professionals in this step.

The fourth step is the final stage, in which the physical model of the cranial prosthesis visualized in the third step is printed. The physical model of the cranial prosthesis is again visually validated before surgery by surgeons to achieve the effect of secondary confirmation. In this study, the details of the printing of the cranial prosthesis are not included in the results and discussion.

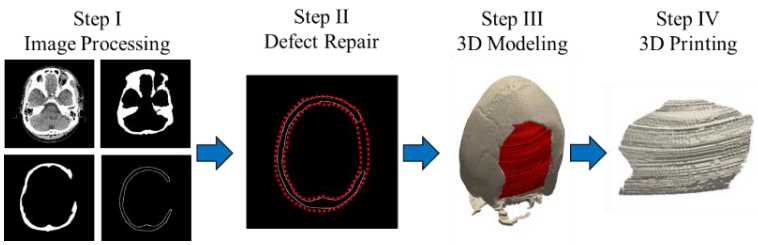

Figure 2 Main steps of the prosthesis reconstruction procedure

(a) (b) (c) (d) (e)

Figure 3 (a) CT slice of the broken skull (b) The edge of the skull (c) Inner border of the skull bone (d) Outer border of the skull bone (e) Example of filling the skull defect

Figure 3 shows the reconstruction method for skull repair in this study. The main purpose of the reconstruction method proposed in this study is to repair the damaged and incomplete skull. The Snakes and DE in this study is used to generate curves of different shapes and compare them with the remaining skull regions. Figure 3(a) to Figure 3(d) are image processing process. First, a binary sample damaged skull is shown in Figure 3(a). The white region in Figure 3(a) represents the remaining skull bone area; in addition, this 2D skull image has a laterally missing white region. Second, we modeled the incomplete skull bone by acquiring the edge of the white region (inner and outer borders), as illustrated in Figure 3(b). Third, in order to increase the accuracy of the experiment, we separately performed the inner and outer border experiments. The inner and outer borders of the skull bone are shown in Figure 3(c) and Figure 3(d), respectively. Finally, our research goal was to use the deformed curves generated by the Snakes and DE to fill the skull defect, as shown in Figure 3(e). Moreover, we performed the inner and outer border separately has an advantage. We can obtain suitable thickness accurate and automatically. We do not need to set an additional parameter like Rudek et al. (2013) to define the thickness.

3.1 Snakes and Thickness Trimming

After acquire and process computed tomography (CT) images in step I as shown in Figure 2. We reconstruct the missing region of the skull bone by using the snake. From the perspective of skull anatomy and past literatures, the curve of the skull in each CT is not exactly the same, but most curves are oval (Rudek et al., 2013). Therefore, the generated curve in each CT can be modeled as being similarly oval with different shapes. Liao et al. (2013) use Snakes and registration in skull reconstruction. But they are mainly used registration in skull modelling process. Snakes is mainly used in image noises elimination not used in skull modelling. In addition, from their study we observe that the feature of Snakes can be used in skull modelling. According to the characteristics of Snakes, the generated curve moves as close as possible to the edge of skull border (inner and outer border). In our study, Snakes can fulfill all requirements of skull modeling. For an outer border example, Figure 4 depicts a schematic

diagram of Snakes. The blue dotted line represents the initial contour in the Snakes, and the red dotted line represents the final suitable contour. The blue dotted line gradually moves toward the red dotted line in the process. Once the initial contour stops moving, the suitable contour in this CT image is found. In order to accelerate the operation speed in the experiment, we suggest that the initial contour be generated as close as possible and surround the skull image.

In the snake process, after we find the snake curve, thickness trimming is the next operation. The thickness of the skull bone in each CT layer is not the same that is another problem that should be considered (Rudek et al., 2011). In this study we do not need to worry thickness problem, we subtracted the outer border from the inner border. Thus, we obtained the thickness of the skull bone in each CT layer automatically. The procedure of thickness trimming is shown in Figure 5. The red dotted line in Figure 5 is the final contour generated by the snake. We fill the final contour of the outer and inner borders with solid graphics, then subtracted the outer border from the inner border. Finally, we obtained a complete skull bone in each CT layer.

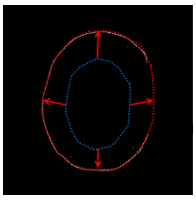

Figure 4 Schematic diagram of a snake sample

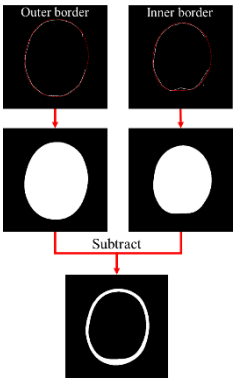

Figure 5 Thickness trimming procedure for every CT layer

3.2 Application of Differential Evolution Algorithm

As discussed in section 2.3, DE was proposed by Storn and Price (1997), is a population-based stochastic search technique. DE has several advantages in heuristic algorithms. It is simpler to perform and has fewer parameters and maintains the diversity of the population. Compared with other EAs (Back et al., 1997), DE is more reliable, performs better, and converges more quickly in solving optimal problems (Hu et al., 2013; Salman et al., 2007). In this study, the combination of mathematical parametric model and heuristic algorithms will be

used to reconstruct the defect skull. We introduce Superellipse as mathematical model and DE to solve this problem. As mentioned in section 2.2, Superellipse can be used to create any geometry commonly found in nature. Our goal is use DE to find suitable parameters of Superellipse so that the resulting curve can be similar to the skull.

After using DE to find a set of parameters, we convert the curve to the CT and determine whether the resulting curve is suitable for the skull. The Superellipse point $E(i,j)$ can be obtained by polar coordinates as shown in Equation (3.1). $E(i,j)$ is the binary value of a pixel in the current position. (i,j) is the position of row and column on the CT image. r value is the result value calculated from the Superellipse as show in Equation (2.1). x_0, y_0 are center coordinates needed to be found by DE.

$$E(i,j) = (r * cos\varphi + x_0, r * sin\varphi + y_0) \tag{3.1}$$

We define a fitness function $F(X)$ to determine whether the resulting curve is suitable or not as shown in Equation (3.2). This fitness function is used to estimate the curve adjustment and can be found in (Rudek, Canciglieri Jr, & Greboge, 2012). Each CT slice of the broken skull is demonstrated as a black-and-white gray scale image. Each point $I(i,j)$ in image I (the CT slice) is the position of one pixel, and its binary value is 1. The l and c values are the total rows and columns, respectively in image I. The concept of fitness function is the ratio of the curve generated by Superellipse covering on the defect skull.

$$F(X) = \frac{\sum_{i=1}^{l}\sum_{j=c}^{c}[I(i,j) * E(i,j)]}{\sum_{i=1}^{l}\sum_{j=c}^{c} I(i,j)} \tag{3.2}$$

All parameters, such as major and minor axis (a, b), number of fixed arguments (m), curvature ($n1$, $n2$, and $n3$) from Equation (2.1) and the center coordinates x_0, y_0, are all generated by the DE algorithm. During the simulation of DE, each new candidate solution is a combination of several individuals in the population. A candidate that obtains a better fitness value than that of the parent individuals replaces the latter.

In order to speed up the overall calculation time and accuracy. Rudek et al. (2011) proposed a limited range to restrict the values in the initial population by specifying the lower and upper bounds. The upper and lower value limits of these parameters can be defined following (Rudek et al., 2011). However, the number of sides of the polygon m and the curvature $n1$,$n2$,$n3$ are not mentioned in (Rudek et al., 2011). Therefore, according to our analysis of the CT image, the upper and lower bounds of the m value are set as 1 and 8, and the $n1$, $n2$, $n3$ values are between 1 and 32. The unit of measurement is pixels.

The concept of using DE and Superellipse is adapted to generate an elliptical shape that

can self-adjust in the skull border. In this study, the principal goal is to determine whether the near optimal arc generated from DE and Superellipse can fit the missing white region and reconstruct the skull in the 2D CT image. The task is to create the most suitable curved shape for this defect skull by tuning the parameters in superellipse. The optimal parameter set will be found by using DE in this study.

Chapter 4 Analyses of Results

We use one originally broken skull from a patient in a real case testing sample in this study and compare the differences between the two methods. We use an originally broken (indicating no bone area) in the lateral region of the skull from a patient in a real case to verify the feasibility of this study. The resolution of the patient CT image is 512 × 512, and this originally broken skull could be transformed into 265 layers. The Snake and DE script are programmed in MATLAB. First, we extracted the skull bone from the CT image (DICOM file format) and identified the inner and outer borders of the skull bone in each layer. Subsequently, according to the skull bone border in Figure 3(c) and Figure 3(d), we used the Snake and DE to fill the skull defect for bone border reconstruction. And then stack all the CT images presented to the medical profession as a 3D visualization model. The experiment was conducted in a 64-bit Win10 system computer with an i7-4720HQ CPU and 8G RAM.

4.1 Analyses of Snake Method

We use Snake to fill the skull defect for bone border reconstruction. The vital parameter values of the Snake are shown in Table 1. Parameter α is a flexible energy value that controls the elastic deformation of the contour. Parameter α is a kind of energy that drives the graph inward. If α is too high, the contour generated by the snake zooms out into a small circle. Therefore, in this case, α was set at 0.1. Kass et al. (1988) reported that if β was set at 0, the snake may become discontinuous and develop a corner. However, to acquire the contour that fit skull border, we required a contour with some slight corners. Accordingly, we set β to be slightly more than zero. v represents the total points of the final snake.

Table 1 Vital parameter values of Snake

Parameter/Snake	Value
α	0.1
β	0.3
v	200

Figure 6(a) to Figure 6(c) are samples of originally broken skull from a patient in a real

case. The Snake parameter settings of these three figures are same as Table 1. Figure 6(a) illustrates the suitable final fitting arc curve in the experiment. The white line represents the whole border of the skull. The red dotted line represents the result curve generated by Snake, and the blue dotted line represents the initial curve of Snake in this layer. Figure 6(b) displays a protruding final fitting arc curve from the experiment. This problem was caused by the initial curve being too far outside from the skull border. A protruding surface affects the appearance of the patient. May cause the patient's head to look asymmetrical. Such a modeling result does not meet our requirements for aesthetics. Figure 6(c) depicts a subsiding final fitting arc curve from the experiment. This problem was caused by the initial curve being too small inside the skull border. A subsiding surface also affects the appearance and symmetry of the patient. This situation does not meet our requirements for aesthetics. From the aforementioned results, the position of the initial curve of Snake is considerably crucial. If the position of the initial curve is chosen wisely and correctly, the final fitting arc curve snake can satisfy our demand. Therefore, we generated the initial curve as close as possible to the skull bone border to avoid the protrusion and subsidence problems.

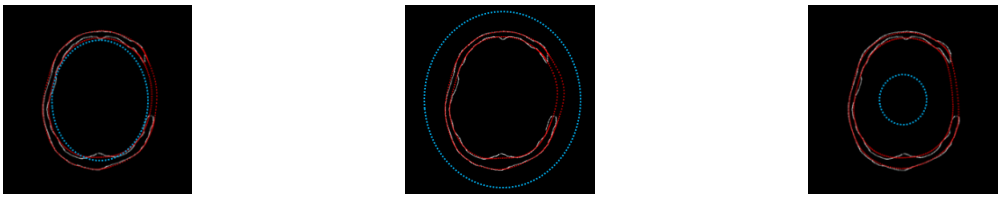

(a) (b) (c)

Figure 6 (a) Suitable final arc curve (b) Protruding final arc curve (c) Subsiding final arc curve

4.2 Analyses of Differential Evolution Algorithm Method

We use an originally broken skull from a patient in a real case as a testing sample in this case. First, we take the same process as Figure 3. We extract the shape of the skull and define the inner and outer border. Then begin to reconstruct the broken skull by using DE algorithm and Superellipse. All the parameter values of DE, as suggested in (Storn & Price, 1997) are shown in Table 2. Each algorithm is performed 30 independent runs. All 30 independent runs parameter values of Superellipse used to fit the inner and outer borders of the skull bone are shown in Table 3 (the numbers represent the average and standard deviation of the experiments).

Table 2 Parameter values of DE algorithm

Parameter/DE	DE/rand1
F	0.5
CR	0.9

NP	64
Dimension	8
Generation	2000

Table 3 Superellipse parameters and fitness function

Superellipse/mean(SD)	Inner border	Outer border
a	145.52 (36.85)	170.98 (24.67)
b	136.57 (32.08)	161.07 (29.11)
m	1.28 (0.51)	1.29 (0.99)
$n1$	18.52 (13.51)	17.13 (14.46)
$n2$	18.35 (13.43)	16.67 (14.09)
$n3$	18.59 (13.62)	17.17 (14.49)
x_0	257.55 (13.15)	249.05 (13.56)
y_0	244.55 (14.43)	254.27 (15.55)
Fitness	0.25 (0.05)	0.26 (0.06)

We choose a sample from the experiments to discuss. Figure 7 demonstrates a fitting arc curve in DE inner-border experiments, and Figure 8 shows a fitting arc curve for DE outer-border experiments. These two Superellipse parameter value are both included in Table 4. We can obtain the solution of this layer by stacking Figure 7 and Figure 8. In order to facilitate the observation, inner and outer fitting arc curve are painted into yellow and red respectively. The yellow line represents the solution of the inner border, and the red line represents the solution of the outer border. After we obtain the solution of inner border and outer border, we integrate these two solutions in a 2D image shown in Figure 9. And there is an advantage why we use inner border and outer border instead of using the whole skull bone in this research. According to the previously mentioned, every thickness of skull bone in each CT layer is not the same. So we need to determine different thickness in a curve additionally according to the shape of specific skull segment. In this study, we can obtain a different thickness curve by using inner border and outer border.

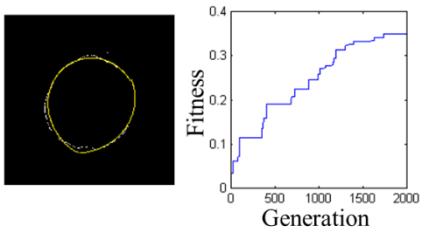

Figure 7 Inner border of DE experiment

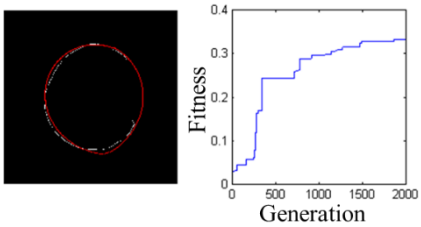

Figure 8 Outer border of DE experiment

Table 4 A sample of Superellipse parameter value

Superellipse parameter	Inner border	Outer border
a	130.73	140.20
b	112.51	141.84
m	1.34	1.23
$n1$	31.64	30.58
$n2$	31.77	30.78
$n3$	31.76	30.34
x_0	264.58	251.33
y_0	246.00	244.30
Fitness	0.35	0.34

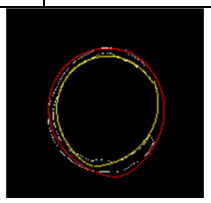

Figure 9 Combination of the inner and outer borders

From the experimental data and observation in Table 3, all the graphs generated by Superellipse have a spherical pattern. This argument can be validated from the results of the execution parameters m, $n1$, $n2$, and $n3$. In this study, the average value of m is 1.28, which is close to 0. (Rudek et al. (2013)) mentioned that a circle can be obtained when parameter m = 0. On the other hand, we found that the average value of $n1$, $n2$, and $n3$ is close to each other. The difference between the three is not obvious. This is also an indicator of spherical tendency when $n1$, $n2$, and $n3$ values are approximate.

4.3 Comparison between Snake and DE Method

Figure 10 and Figure 11 are the result of 265 layers originally broken skull from a patient in a real case. We stacked the skull and the prosthesis CT in the same space. Then we can obtain the result of our experiment. White part is the skull bone and the red part is the prosthesis. We can let the professional medical staff assess prosthesis before we print out the 3D prosthesis. The surface using the Snake method is smoother than the surface using the DE method. Overall, both methods can fill the broken skull into a complete appearance.

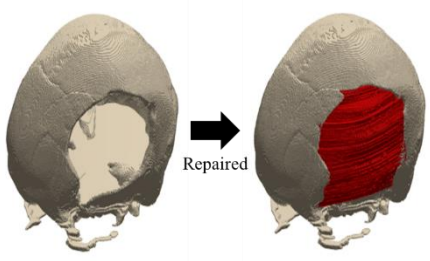

Figure 10 Skull repairing result of Snake method

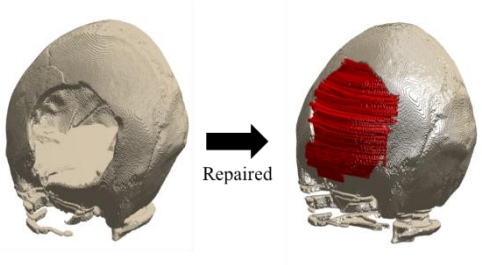

Figure 11 Skull repairing result of DE method

The objective of these methods is to find a cranial curve with a suitable fit by using defect repairing algorithm. However, a curve with a suitable fit might still have some issues in regard to the junction points between real and fitted curves, as shown in Figure 12. A part that is framed by a blue rectangle has marked out the problem. In this case, neither the inner nor the outer borders are one hundred percent aligned with the contact points of the inner and outer borders.

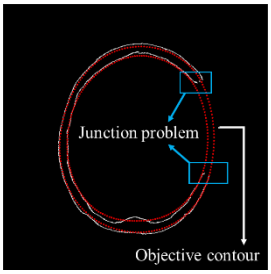

Figure 12 Example of junction problem

Chapter 5 Conclusion and Future Work

Skull defects result in adverse psychological or physical effects for patients, such as low protection of the brain, a high risk of brain infection, social barrier, and inferiority. Moreover, skull defects affect the aesthetic appearance and cause the appearance of the head asymmetry. Cranioplasty is a common method used to reconstruct the integrity of the cranial cavity and protecting the brain from external force. This paper presents two methods of prosthesis modeling by using a snake and DE. The main goal of both approaches is developed optimal self-adjusting bone curvature algorithm that can automatically generate a suitable curve in the broken skull part. The experiments validated the proposed methods, which could build a prosthesis model of a broken skull bone (notch in the skull). The significant contribution of this work is that Snake and DE can be used to model an arc curve for which information does not exist in the image without making prosthesis manually. The proposed method can also save a lot of time for the manufacture of a precise prosthesis for surgeons because they do not need to manually build the prosthesis. The patient does not have to spend a lot of time waiting in the operating room. Thus, the proposed method is a promising technique for medical professionals those who need to solve geometric prosthesis modeling problems. We demonstrate the feasibility of these methods from the experimental results. We believe that the proposed method is a convenient and efficient strategy that can be used by medical professionals to reconstruct the skull bone defects of patients. However, the junction problem as mentioned in section 4.3 is still need to be improved. Junction points between the defect bone segments and the objective contour must be solved in future studies.

References

Aarabi, B., Hesdorffer, D. C., Ahn, E. S., Aresco, C., Scalea, T. M., & Eisenberg, H. M. (2006). Outcome following decompressive craniectomy for malignant swelling due to severe head injury. *Journal of neurosurgery, 104*(4), 469-479.

Back, T., Fogel, D. B., & Michalewicz, Z. (1997). *Handbook of evolutionary computation*: IOP Publishing Ltd.

Black, S. (1978). Reconstruction of the supraorbital ridge using aluminum. *Surgical neurology, 9*(2), 121-128.

Carr, J. C., Fright, W. R., & Beatson, R. K. (1997). Surface interpolation with radial basis functions for medical imaging. *IEEE transactions on medical imaging, 16*(1), 96-107.

Chong, C. S., Lee, H., & Kumar, A. S. (2006). Automatic hole repairing for cranioplasty using Bézier surface approximation. *Journal of Craniofacial Surgery, 17*(2), 344-352.

Cooper, D. J., Rosenfeld, J. V., Murray, L., Arabi, Y. M., Davies, A. R., D'urso, P., . . . Reilly,

P. (2011). Decompressive craniectomy in diffuse traumatic brain injury. *New England Journal of Medicine, 364*(16), 1493-1502.

Davis, L. (1991). Handbook of genetic algorithms.

Dean, D., & Min, K.-J. (2003). *Deformable templates for preoperative computer-aided design and fabrication of large cranial implants.* Paper presented at the International Congress Series.

Deramond, H., Wright, N., & Belkoff, S. M. (1999). Temperature elevation caused by bone cement polymerization during vertebroplasty. *Bone, 25*(2), 17S-21S.

Ghadimi, S., Moghaddam, H. A., Grebe, R., & Wallois, F. (2016). Skull segmentation and reconstruction from newborn CT images using coupled level sets. *IEEE journal of biomedical and health informatics, 20*(2), 563-573.

Gielis, J. (2003). A generic geometric transformation that unifies a wide range of natural and abstract shapes. *American journal of botany, 90*(3), 333-338.

Gooch, M. R., Gin, G. E., Kenning, T. J., & German, J. W. (2009). Complications of cranioplasty following decompressive craniectomy: analysis of 62 cases. *Neurosurgical focus, 26*(6), E9.

Greboge, T., Grebogi, R. B., Rudek, M., & Canciglieri Jr, O. (2011). *Geometric Prosthesis Modeling to Skull Repairing Using Artificial Intelligence Methods.* Paper presented at the 41st International Conference on Computers & Industrial Engineering (CIE 41), Los Angeles.

Greboge, T., Rudek, M., Jahnen, A., & Júnior, O. C. (2013). *Improved Engineering Design Strategy Applied to Prosthesis Modelling.* Paper presented at the ISPE CE.

Gruber, R., Peter, R., & Hora, J. (1988). The prognosis of cranioplasty following large craniectomy in children. *Zeitschrift für Kinderchirurgie, 43*(06), 375-383.

Hu, Z., Xiong, S., Su, Q., & Zhang, X. (2013). Sufficient conditions for global convergence of differential evolution algorithm. *Journal of Applied Mathematics*.

Huang, G.-y., & Shan, L.-j. (2011). *Research on the Digital Design and Manufacture of Titanium Alloy Skull Repair Prosthesis.* Paper presented at the Bioinformatics and Biomedical Engineering.

Jiranek, W. A., Hanssen, A. D., & Greenwald, A. S. (2006). Antibiotic-loaded bone cement for infection prophylaxis in total joint replacement. *J Bone Joint Surg Am, 88*(11), 2487-2500.

Josan, V., Sgouros, S., Walsh, A., Dover, M., Nishikawa, H., & Hockley, A. (2005). Cranioplasty in children. *Child's Nervous System, 21*(3), 200-204.

Junior, O. C., Rudek, M., & Greboge, T. (2011). A prosthesis design based on genetic algorithms in the concurrent engineering context *Improving Complex Systems Today* (pp. 241-248): Springer.

Kass, M., Witkin, A., & Terzopoulos, D. (1988). Snakes: Active contour models. *International journal of computer vision, 1*(4), 321-331.

Kennedy, J. (2010). Particle swarm optimization *Encyclopedia of Machine Learning* (pp. 760-

766): Springer.

Kuo, J.-R., Wang, C.-C., Chio, C.-C., & Cheng, T.-J. (2004). Neurological improvement after cranioplasty–analysis by transcranial Doppler ultrasonography. *Journal of Clinical Neuroscience, 11*(5), 486-489.

Lewis, G. (1997). Properties of acrylic bone cement: state of the art review. *Journal of biomedical materials research, 38*(2), 155-182.

Li, H., Xie, Z., Ruan, S., & Wang, H. (2009). The measurement and analyses of symmetry characteristic of human skull based on CT images. *Journal of Biomedical Engineering, 26*(1), 34-37.

Liacouras, P., Garnes, J., Roman, N., Petrich, A., & Grant, G. T. (2011). Designing and manufacturing an auricular prosthesis using computed tomography, 3-dimensional photographic imaging, and additive manufacturing: a clinical report. *The Journal of prosthetic dentistry, 105*(2), 78-82.

Liao, Y.-L., Lu, C.-F., Sun, Y.-N., Wu, C.-T., Lee, J.-D., Lee, S.-T., & Wu, Y.-T. (2011). Three-dimensional reconstruction of cranial defect using active contour model and image registration. *Medical & biological engineering & computing, 49*(2), 203-211.

Liao, Y.-L., Lu, C.-F., Wu, C.-T., Lee, J.-D., Lee, S.-T., Sun, Y.-N., & Wu, Y.-T. (2013). Using three-dimensional multigrid-based snake and multiresolution image registration for reconstruction of cranial defect. *Medical & biological engineering & computing, 51*(1-2), 89-101.

Liebschner, M. A., Rosenberg, W. S., & Keaveny, T. M. (2001). Effects of bone cement volume and distribution on vertebral stiffness after vertebroplasty. *Spine, 26*(14), 1547-1554.

Maravelakis, E., David, K., Antoniadis, A., Manios, A., Bilalis, N., & Papaharilaou, Y. (2008). Reverse engineering techniques for cranioplasty: a case study. *Journal of medical engineering & technology, 32*(2), 115-121.

Plum, A. W., & Tatum, S. A. (2015). A comparison between autograft alone, bone cement, and demineralized bone matrix in cranioplasty. *The Laryngoscope, 125*(6), 1322-1327.

Prolo, D. J., & Oklund, S. A. (1991). The use of bone grafts and alloplastic materials in cranioplasty. *Clinical orthopaedics and related research, 268*, 270-278.

Rish, B. L., Dillon, D. J., Meirowsky, A. M., Caveness, W. F., Mohr, J. P., Kistler, P. J., & Weiss, G. H. (1979). Cranioplasty: a review of 1030 cases of penetrating head injury. *Neurosurgery, 4*(5), 381-385.

Rudek, M., Canciglieri Jr, O., & Greboge, T. (2012). *An Optimized Method for Anathomic Skull Prosthesis Modelling.* Paper presented at the 13Th IASTED Conference in Computer Graphics and Image, CGIM2012, Crete-Greece.

Rudek, M., Canciglieri Jr, O., & Greboge, T. (2013). A PSO Application in Skull Prosthesis Modelling by Superellipse. *ELCVIA Electronic Letters on Computer Vision and Image Analysis, 12*(2).

Rudek, M., Greboge, T., Coelho, L. d. S., & Canciglieri Jr, O. (2011). *Using Genetic*

Algorithms to Support the Prosthesis Design in the CAD System. Paper presented at the Proceedings of the 21st Brazilian Congress of Mechanical Engineering COBEM 2011.

Rudek, M., Gumiel, Y. B., & Canciglieri Jr, O. (2015). Autonomous CT replacement method for the skull prosthesis modelling. *Facta Universitatis, Series: Mechanical Engineering, 13*(3), 283-294.

Sahillioğlu, Y., & Kavan, L. (2015). Skuller: A volumetric shape registration algorithm for modeling skull deformities. *Medical image analysis, 23*(1), 15-27.

Salman, A., Engelbrecht, A. P., & Omran, M. G. (2007). Empirical analysis of self-adaptive differential evolution. *European Journal of operational research, 183*(2), 785-804.

Sanan, A., & Haines, S. J. (1997). Repairing holes in the head: a history of cranioplasty. *Neurosurgery, 40*(3), 588-603.

Sengupta, D. P., Sengupta, D., & Ghosh, P. (2005). Bilaterally symmetric Fourier approximations of the skull outlines of temnospondyl amphibians and their bearing on shape comparison. *Journal of biosciences, 30*(3), 377-390.

Spehr, M., Gumhold, S., & Fleming, R. W. (2011). Sum-of-Superellipses–A Low Parameter Model for Amplitude Spectra of Natural Images *Image Analysis and Processing–ICIAP 2011* (pp. 128-138): Springer.

Storn, R., & Price, K. (1997). Differential evolution–a simple and efficient heuristic for global optimization over continuous spaces. *Journal of global optimization, 11*(4), 341-359.

Taggard, D. A., & Menezes, A. H. (2001). Successful use of rib grafts for cranioplasty in children. *Pediatric neurosurgery, 34*(3), 149-155.

Viterbo, F., Palhares, A., & Modenese, E. (1995). Cranioplasty: the autograft option. *Journal of Craniofacial Surgery, 6*(1), 80-82.

Wagner, M. E. H., Lichtenstein, J. T., Winkelmann, M., Shin, H.-o., Gellrich, N.-C., & Essig, H. (2015). Development and first clinical application of automated virtual reconstruction of unilateral midface defects. *Journal of Cranio-Maxillofacial Surgery, 43*(8), 1340-1347.

Winkler, P. A., Stummer, W., Linke, R., Krishnan, K. G., & Tatsch, K. (2000). Influence of cranioplasty on postural blood flow regulation, cerebrovascular reserve capacity, and cerebral glucose metabolism. *Journal of neurosurgery, 93*(1), 53-61.

Zhang, X., & Rosin, P. L. (2003). Superellipse fitting to partial data. *Pattern Recognition, 36*(3), 743-752.

Zhang, Z., Zhang, R., & Song, Z. (2014). Skull defect reconstruction based on a new hybrid level set. *Bio-medical materials and engineering, 24*(6), 3343-3351.

Zhou, L., Song, Y., Wu, J., Li, H., Zhang, G., & Sun, C. (2013). Surface Reconstruction of Bilateral Skull Defect Prosthesis Based on Radial Basis Function *Informatics and Management Science I* (pp. 741-747): Springer.